The Dynamic Impact Experiments Under Active Confining Pressure and the Constitutive Equation of PP/PA Blends at Multi-Axial Compressive Stress State

Shi Shaoqiu, Yu Bing, Wang Lili*

Summary: A special active hydraulic confining pressure installation matched with Φ14.5 mm SHPB apparatus was developed. A series of active confining pressure impact experiments for PP/PA blends are performed in this special SHPB system under two kinds of axial strain rate: $8.0^{*}10^{2}$, $1.4^{*}10^{3}\ s^{-1}$ and the active confining pressure of 0 MPa, 4 MPa, 8 MPa, 12 MPa, 15 MPa, 20 MPa. The axial strain-time profile, the axial stress-time profile and the hoop strain-time profile of the specimen are recorded online respectively. According to the equilibrium equation, the complete state of principal stress and principal strain of PP/PA blends under multi-axial stress state is analyzed. The experimental results reveal that the axial stress-strain curves all are related to the confining pressure and the strain rate. It can also be seen that under a constant effective strain rate the effective stress- effective strain curves at different confining pressures are coincident basically. This manifests that under a certain effective strain rate there is only one unique effective stress- effective strain curve. The multi-axial constitutive equation for PP/PA blends is suggested finally as:

$$\underline{\sigma} = (\sigma_{\text{conf.}} + \sigma_{\text{eff}}/3)\underline{\mathbf{I}} + \underline{\mathbf{A}}\sigma_{\text{eff}}$$

where σ_{conf} is the confining pressure value.

$$\sigma_{eff}(\varepsilon_{eff}, \dot{\varepsilon}_{eff}) = E\varepsilon_{eff} + \alpha\varepsilon_{eff}^{2} + \beta\varepsilon_{eff}^{3} + E_2 \int_0^t \dot{\varepsilon}_{eff}(\tau) \exp\left(-\frac{t-\tau}{\theta_2}\right) d\tau$$

For 113 PP/PA blends, $E = 2.98$ GPa, $\alpha = -31.15$ GPa, $\beta = 93.31$ GPa, $\theta_2 = 8.54$ μS, $E_2 = 0.82$ GPa.

Keywords: active confining pressure; blends; high strain rate; multi-axial constitutive equation; SHPB

Introduction

Most polymer structures in service always undergo various kinds of impact loadings. Because of their inertia and all kinds of confined constraints they are sustained, they are always under multi-axial and high strain rate conditions. In order to guarantee the safe design of these polymer structures, the impact dynamic response of these materials under multi-axial stress state should be known. In the last 2 decades, the quantity of multi-axial investigations for polymers has grown, but most of the multi-axial tests have been carried out under quasi-static conditions usually. The Split Hopkinson Bar Technique (SHBT) is used for the investigation of dynamic responses of polymers under high strain rates. But most of them were restricted in simple loading conditions, such as in compression, tension or shearing, the specimens were really in mono-axial stress state.

Faculty of Engineering, Ningbo University, Ningbo, 315211, P.R. China
E-mail: shishaoqiu@nbu.edu.cn

In this paper, a special active hydraulic confining pressure installation matched with Φ14.5 mm SHPB apparatus was developed. The dynamic impact response of PP/PA blends is tested under two kinds of axial strain rate ($8.0^{*}10^{2}\,s^{-1}$, $1.4^{*}10^{3}\,s^{-1}$) and the active confining pressure from 0 MPa up to 20 MPa. The complete state of stress and strain in the specimen impact loaded is determined through direct experimental measurement. The experimental results reveal that the axial stress-strain curves all are related to the confining pressure and the strain rate. The multi-axial constitutive equation of PP/PA blends under high strain rate is finally described.

Specimen and Testing Equipment

The specimen is made of PP/PA blends with a compatibilizer (grafted thermoplastic elastomer, TPE-g). The weight ratio is PP/PA/TPE-g: 49:30:21. They are called 113 for short. All materials used were dried in ovens for 8 h, at 80 °C. Then cylindrical specimens in diameter of 14.5 mm and length of 10 mm were prepared from injection mold at 210 °C.

A special active hydraulic confining pressure installation matched with 14.5 mm SHPB apparatus was developed in Ningbo University. A high pressure vessel fully filled with silicon oil is matched and installed in Φ14.5 mm SHPB system. Its photo is shown in Figure 1 (a). The oil pressure value inside this vessel can be controlled by a hydraulic pressure control system, in which the maximum acting pressure value can be up to 50 MPa. The photo of this control system is shown in Figure 1 (b).

The knotty difficulties of these acting confining impact tests are encountered in two aspects. The first one is the dynamic leaking of oil under high pressure during the movement of the pressure bars through the hole of the vessel. This problem disables the test to reach the high confining pressure value. We use the O type rubber seals to solve this problem easily. But in many tests, the hole for the passing of the cable linking to the strain gauge on the surface of the specimen was always oil leaked and so that the high confining pressure value can't be reached. Although this hole is sealed by epoxy resin, this difficulty still exists because of the gap between the shielded wire and the cable. We improved the design of the sealing of this local part by using the small O type rubber seal ring instead of epoxy resin. This problem is solved finally. The magnified figure of this structure is shown in Figure 2. The second difficulty of the tests is that the specimen loses contact with pressure bars due to the entering of the high pressure oil into the mini gap between

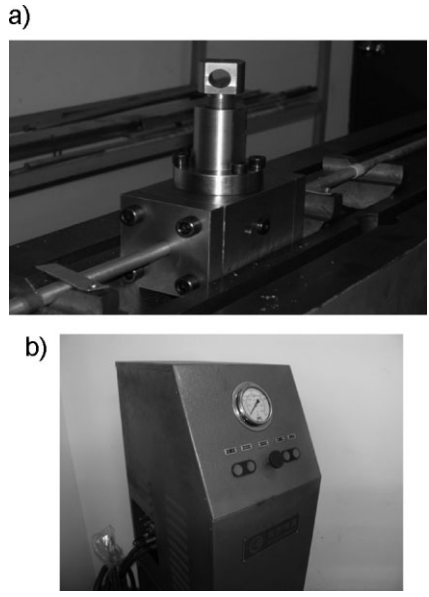

Figure 1.
(a) The active confining pressure installation matched with 14.5 mm SHPB apparatus. (b) The hydraulic pressure control system.

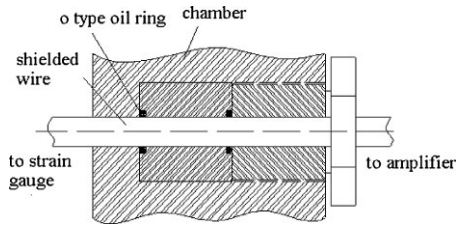

Figure 2.
The structure of the O type rubber ring between the shielded wire and the chamber.

the specimen surface and the bar surface, even though the diameter is the same for the specimen and bars. We use a thermo plastic tube to assemble the specimen and the bars together. Then this thermo plastic tube is heated. It contracts to bound them and shields them from the oil. The separating of the specimen from bars can also be monitored by using the incident and the transmitted stress wave profiles. When the incident and the transmitted bars are not pushed away with the specimen, the difference of time between the initial part of the incident stress wave and the transmitted stress wave should be L/C_0 (L is the distance between the strain gauges on the incident bar and the transmitted bar, C_0 is the wave speed in bars). In our tests, $L = 1\,m$, $C_0 = 5190\,m/s$, this difference of time is about 200 μs. The separating and un-separating cases are shown in Figure 3.

Experimental Part

A series of active confining pressure impact experiments for 113 PP/PA blends are performed in our special SHPB system under two kinds of axial strain rate: $8.0^{*}10^{2}$, $1.4^{*}10^{3}s^{-1}$ and the active confining pressure of 0 MPa, 4 MPa, 8 MPa, 12 MPa, 15 MPa, 20 MPa. The specimen is deformed under both the axial dynamic loading and the active confining pressure around its cylindrical surface. The axial stress-time and the axial strain-time wave profiles are obtained from the strain gauges on the incident and the transmitted bars. The radical stress is just the confining pressure. The hoop strain-time profile ε_θ is measured from a large measuring range strain gauge glued on the specimen. Furthermore, equilibrium equation requires that the radical and hoop stress components at $r = a$ be equal: $\sigma_r(a) = \sigma_\theta(a)$. Corresponding, we have $\varepsilon_r(a) = \varepsilon_\theta(a)$. Thus in our experiments the measurements provide a complete determination of the dynamic stress components as well as the corresponding strain components.

We compare the experimental results under different confining pressures but under the same strain rate. The comparison of their axial stress-strain curves is shown in Figure 4 (axial strain rate $\dot{\varepsilon} = 1.4 * 10^3 s^{-1}$) and in Figure 5 (axial strain rate $\dot{\varepsilon} = 8.0 * 10^2 s^{-1}$). The comparison of the axial stress-strain curves at the same confining pressure but at different axial strain rates is shown in Figure 6 (confining pressure = 8 MPa) and in Figure 7 (confining pressure = 20 MPa).

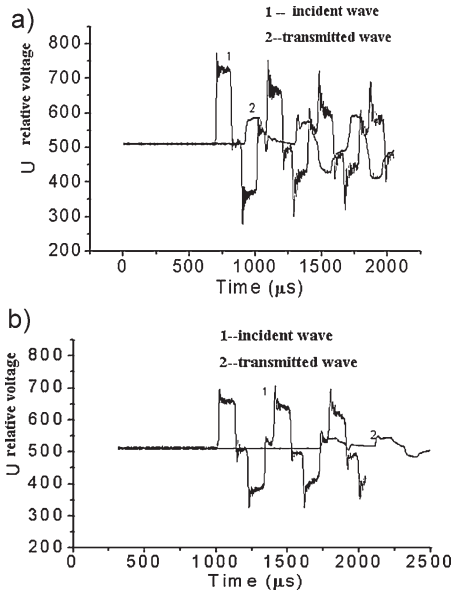

Figure 3.
(a) The monitored wave profiles of un-separating case. (b) The monitored wave profiles of separating case.

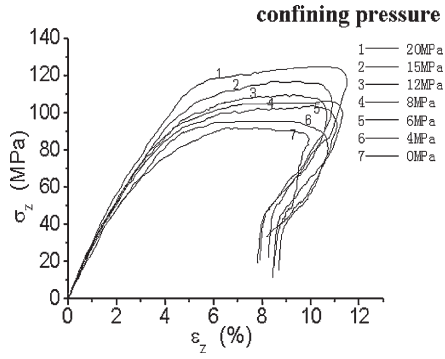

Figure 4.
The comparison of the axial stress-strain curves under different confining pressures at a axial strain rate $\dot{\varepsilon} = 1.4 * 10^3 s^{-1}$.

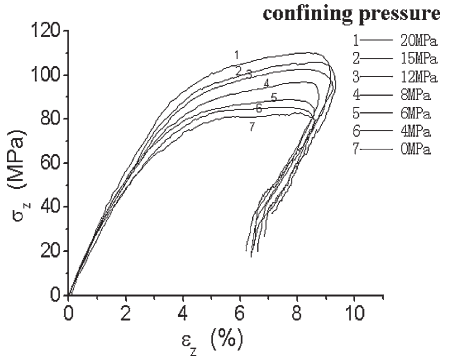

Figure 5.
The comparison of the axial stress-strain curves under different confining pressures at a axial strain rate $\dot{\varepsilon} = 8.0 * 10^2 s^{-1}$.

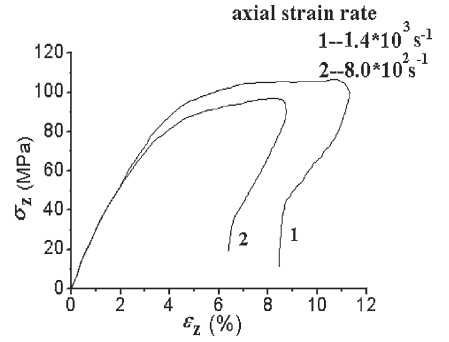

Figure 6.
The comparison of the axial stress-strain curves at different axial strain rate under the confining pressure 8 MPa.

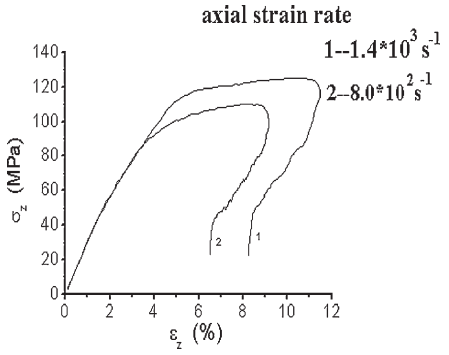

Figure 7.
The comparison of the axial stress-strain curves at different axial strain rate under the confining pressure 20 MPa.

From Figure 4 and Figure 5, we can see that the impact axial response of this 113 material is dependent on the active confining pressure. When the confining pressure is increasing, the stress value corresponding to a certain strain is also increasing and the impact softening phenomenon has weakened. This may be the suppression to the damage evolution of the material at high confining pressure.

From Figure 6 and Figure 7, we can also see that at the confining pressure condition the impact response of 113 materials is still sensitive to the strain rate. When strain rate is increasing, the stress value corresponding to a certain strain is also increasing.

The effective stress and effective strain at the infinitesimal element of the specimen is:

$$\sigma_{eff} = \frac{\sqrt{2}}{2}\sqrt{(\sigma_z-\sigma_r)^2+(\sigma_r-\sigma_\theta)^2+(\sigma_\theta-\sigma_z)^2}$$
$$\varepsilon_{eff} = \frac{\sqrt{2}}{3}\sqrt{(\varepsilon_z-\varepsilon_r)^2+(\varepsilon_r-\varepsilon_\theta)^2+(\varepsilon_\theta-\varepsilon_z)^2} \quad (1)$$

As $\boldsymbol{\sigma}_r(a) = \boldsymbol{\sigma}_\theta(a), \boldsymbol{\varepsilon}_r(a) = \boldsymbol{\varepsilon}_\theta(a)$, equation (1) can be simplified to:

$$\sigma_{eff} = \sigma_z - \sigma_r$$
$$\varepsilon_{eff} = \frac{2}{3}(\varepsilon_z - \varepsilon_r) \quad (2)$$

By differentiating equation (2), we can get:

$$\dot{\varepsilon}_{eff} = \frac{d\varepsilon_{eff}}{dt} = \frac{2}{3}\left(\frac{\partial\varepsilon_{eff}}{\partial\varepsilon_z}\cdot\frac{d\varepsilon_z}{dt} - \frac{\partial\varepsilon_{eff}}{\partial\varepsilon_r}\cdot\frac{d\varepsilon_r}{dt}\right)$$
$$= \frac{2}{3}(\dot{\varepsilon}_z - \dot{\varepsilon}_r) \quad (3)$$

We can use equation (2) to calculate the effective stress and effective strain and use equation (3) to calculate the effective strain rate. Thus the effective stress- effective strain curves at different confining pressures under a constant effective strain rate can be obtained. They are shown in Figure 8 and in Figure 9. We can see that under a constant effective strain rate the effective stress- effective strain curves at different confining pressures are coincident basically. This manifests that under a certain effective strain rate there is only one unique effective stress- effective strain curve. Thus at a constant temperature, the effective stress

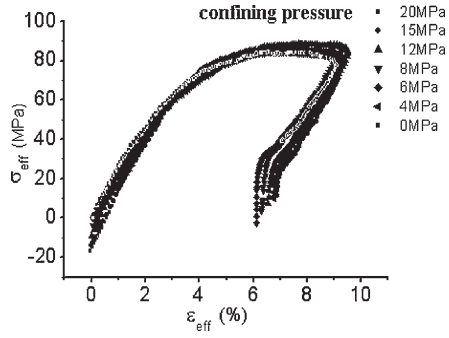

Figure 8.
Effective stress-strain curves under different confining pressure at effective strain rate of 1250 s^{-1}.

σ_{eff} is only a function of the effective strain ε_{eff} and the effective strain rate $\dot{\varepsilon}_{eff}$. That is $\sigma_{eff}(\varepsilon_{eff}, \dot{\varepsilon}_{eff})$.

We can fit the effective stress $\sigma_{eff}(\varepsilon_{eff}, \dot{\varepsilon}_{eff})$ by using ZWT nonlinear visco-elastic equation:[8]

$$\sigma_{eff}(\varepsilon_{eff}, \dot{\varepsilon}_{eff}) = E_0\varepsilon_{eff} + \alpha\varepsilon_{eff}^2 + \beta\varepsilon_{eff}^3 + E_1\int_0^t \dot{\varepsilon}_{eff}(\tau)\exp\left(-\frac{t-\tau}{\theta_1}\right)d\tau + E_2\int_0^t \dot{\varepsilon}_{eff}(\tau)\exp\left(-\frac{t-\tau}{\theta_2}\right)d\tau \quad (4)$$

Under the impact loading with time scale from 1 to $10^2\,\mu s$, the low frequency Maxwell element with the relaxation time θ_1 of 1 to 10^2s has no enough time for relaxation. Then the low frequency Maxwell element is reduced to a single spring element with the elastic constant E_1, and correspondingly, the ZWT nonlinear visco-elastic equation (4) is reduced to

$$\sigma_{eff}(\varepsilon_{eff}, \dot{\varepsilon}_{eff}) = E\varepsilon_{eff} + \alpha\varepsilon_{eff}^2 + \beta\varepsilon_{eff}^3 + E_2\int_0^t \dot{\varepsilon}_{eff}(\tau)\exp\left(-\frac{t-\tau}{\theta_2}\right)d\tau \quad (5)$$

The comparison of the effective stress-effective strain curves under different effective strain rates is shown in Figure 10. In Figure 10, curve 1 is the mean effective stress- effective strain curve of the curves at different confining pressures but at the same effective strain rate $2.2^*10^3 s^{-1}$, curve 2 is the mean effective stress- effective strain curve of the curves at different confining pressures but at the same effective strain rate $1.25^*10^3 s^{-1}$.

By the best least-squares fit, we can get:

$$E = 2.98\,GPa,\ \alpha = -31.15\,GPa,$$
$$\beta = 93.31\,GPa,\ \theta_2 = 8.54\mu s,$$
$$E_2 = 0.82\,GPa$$

The 3-Dimensional Constitutive Equation of PP/PA Blends

When the unloading process is not considered, the deformation is separated into

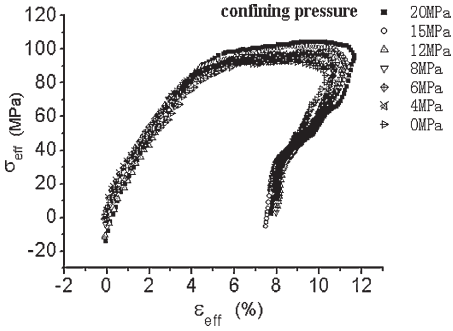

Figure 9.
Effective stress-strain curves under different confining pressure at effective strain rate of 2200 s^{-1}.

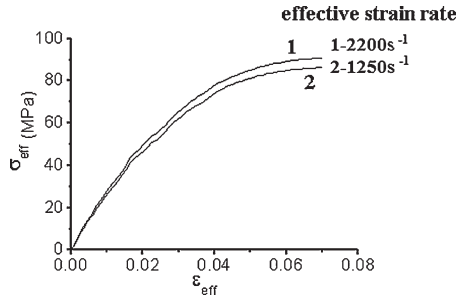

Figure 10.
The comparison of effective stress - effective strain curves under different effective strain rate.

dilatational and distortional parts with the constitutive representation given by

$$\left.\begin{aligned}\sigma_m &= K(\theta)\theta \\ \tau_e &= g(\gamma_e)\gamma_e\end{aligned}\right\} \tag{6}$$

Where σ_m is the mean stress, τ_e is the effective shear stress, θ is the dilatation and γ_e is the effective shear strain. These quantities are defined as follows:

$$\sigma_m = \frac{1}{3}\sigma_{kk},\ \tau_e = \sqrt{\frac{1}{2}s_{ij}s_{ij}},\ \theta = \frac{\Delta V}{V} = \varepsilon_{kk} \text{ and } \gamma_e = \sqrt{e_{ij}e_{ij}}, \tag{7}$$

where e_{ij} are the deviatoric strain components. $K(\theta)$ and $g(\gamma_e)$ represent the bulk and shear constitutive response of the material, respectively. In the linear elastic regime, they become the bulk and shear modulus, respectively.

From the experimental results of three principal stresses and three principal strains for PP/PA blends, the mean stress σ_m-time profile and the dilatation $\frac{\Delta V}{V}$ time profile can be obtained. Then the parameter t is eliminated. The curve of σ_m versus $\frac{\Delta V}{V}$ is obtained and shown in Figure 11, which is in the elastic region and under the effective strain rate of $2.2^{*}10^{3}s^{-1}$. It can be seen that the initial slope $K(\theta)$ of the mean stress variation with the volume dilatation gives the bulk modulus and nearly be a constant for 113 materials.

In our tests, the hoop stress $\boldsymbol{\sigma}_\theta$ *(a)* is equal to the radical stress $\boldsymbol{\sigma}_r$ *(a)*, and $\sigma_m = \frac{1}{3}(\sigma_r + \sigma_\theta + \sigma_z)$. Note: $\sigma_r = \sigma_\theta = \sigma_{conf.}$, we can get:

$$\left.\begin{aligned}\sigma_r &= \sigma_{m.} - \frac{\sigma_z - \sigma_{conf.}}{3} \\ \sigma_\theta &= \sigma_m - \frac{\sigma_z - \sigma_{conf.}}{3} \\ \sigma_z &= \sigma_m + \frac{2(\sigma_z - \sigma_{conf.})}{3}\end{aligned}\right. \tag{8}$$

Because of $\boldsymbol{\sigma} = \begin{bmatrix}\sigma_r & 0 & 0\\ 0 & \sigma_\theta & 0\\ 0 & 0 & \sigma_z\end{bmatrix} = \begin{bmatrix}\sigma_m & 0 & 0\\ 0 & \sigma_m & 0\\ 0 & 0 & \sigma_m\end{bmatrix}$

$$+\begin{bmatrix}\sigma_r - \sigma_m & 0 & 0\\ 0 & \sigma_\theta - \sigma_m & 0\\ 0 & 0 & \sigma_z - \sigma_m\end{bmatrix},$$

Combining equation (2) and equation (8), the effective stress deviatoric components τ_e can be expressed as:

$$\tau_e = \begin{bmatrix}-\frac{1}{3} & 0 & 0\\ 0 & -\frac{1}{3} & 0\\ 0 & 0 & \frac{2}{3}\end{bmatrix}\sigma_{eff} \tag{9}$$

Combining equation (2) and $\sigma_m = \frac{1}{3}(\sigma_r + \sigma_\theta + \sigma_z)$, we can get:

$$\sigma_m = \sigma_{conf.} + \frac{\sigma_{eff}}{3} \tag{10}$$

So a constitutive equation at multi-axial stress state under high strain rate for PP/PA blends is finally described as:

$$\underline{\sigma} = (\sigma_{conf.} + \sigma_{eff}/3)\underline{\mathbf{I}} + \underline{\mathbf{A}}\sigma_{eff} \tag{11}$$

where

$$\mathbf{A} = \begin{bmatrix}-\frac{1}{3} & 0 & 0\\ 0 & -\frac{1}{3} & 0\\ 0 & 0 & \frac{2}{3}\end{bmatrix}$$

$$\sigma_{eff}(\varepsilon_{eff}, \dot{\varepsilon}_{eff}) = E\varepsilon_{eff} + \alpha\varepsilon_{eff}^2 + \beta\varepsilon_{eff}^3 + E_2\int_0^t \dot{\varepsilon}_{eff}(\tau)\exp\left(-\frac{t-\tau}{\theta_2}\right)d\tau,$$

For 113 blends, $E = 2.98GPa$, $\alpha = -31.15\,GPa$, $\beta = 93.31\,GPa$, $\theta_2 = 8.54\,\mu S$, $E_2 = 0.82\,GPa$.

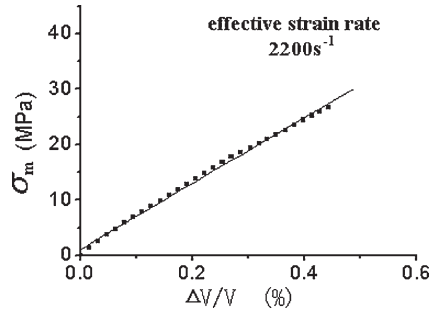

Figure 11.
The curve of σ_m versus $\frac{\Delta V}{V}$.

Conclusion

By using a special active hydraulic confining pressure installation matched with 14.5 mm SHPB apparatus, the dynamic impact response of PP/PA blends is tested under

different axial strain rate and different confining pressure. The axial strain-time profile, the axial stress-time profile and the hoop strain-time profile of the specimen are recorded online respectively. According to the equilibrium equation, the complete state of principal stress and principal strain of PP/PA blends under multi-axial stress state is analyzed.

The experimental results reveal that the axial stress-strain curves all are related to the confining pressure and the strain rate. The multi-axial constitutive equation for PP/PA blends is suggested finally as:

$$\underline{\sigma} = (\sigma_{\text{conf.}} + \sigma_{\text{eff}}/3)\underline{\mathbf{I}} + \underline{\mathbf{A}}\sigma_{\text{eff}}$$

where σ_{conf} is the confining pressure value.

$$\sigma_{eff}(\varepsilon_{eff}, \dot{\varepsilon}_{eff}) = E\varepsilon_{eff} + \alpha\varepsilon_{eff}^2 + \beta\varepsilon_{eff}^3 + E_2 \int_0^t \dot{\varepsilon}_{eff}(\tau) \exp\left(-\frac{t-\tau}{\theta_2}\right) d\tau$$

For 113 PP/PA blends, $E = 2.98\,GPa$, $\alpha = -31.15\,GPa$, $\beta = 93.31\,GPa$, $\theta_2 = 8.54\,\mu S$, $E_2 = 0.82\,GPa$.

Acknowledgements: This paper is sponsored by K.C. Wong Magna Fund in Ningbo University. The support of the National Natural Science Foundation of China (No.10372046) is deeply appreciated.

[1] J. D. Ferry, *Viscoelastic Properties of Polymers*, Wiley, New York 1980.
[2] W. Chen, G. Ravichandran, "An Experimental Technique for Imposing Dynamic Multiaxial Compression with Mechanical Confinement'. *Experimental Mechanics*, *36*, **1996**, 155–158.
[3] Z. Ma, K. Ravi-Chandar, Confined Compression: A Stable Homogeneous Deformation for Constitutive Characterization. *Experimental Mechanics 40*(1), March **2000**, 38–45.
[4] N. R. Karttunen, A. J. Lesser, "Modeling the Yield Behavior of an Aliphatic Polyketone in Multi-axial Stress States". *Polymer Engineering & Structure*, *40*(11), **2000**.
[5] W. Chen, "Electro-magnetic Confinement for Dynamic Multiaxial Compression Experiments'. *Experimental Tech. 23*, **1999**, 24–26.
[6] Shi Shaoqiu, Gansu, Wang Lili, The Thermo-Viscoelastic Mechanical Behavior of Aeronautical PMMA under Impact Loading. *Journal of Ningbo University*, 1, **1988**, No., 58–68.
[7] Wang Lili, Zhu Xixiong, Shi Shaoqiu, An Impact Dynamics Investigation on some Problems in Bird Strike on Windshields of High Speed Aircraft. *Acta Aeronautica et Astronautica Sinica*, *5*, **1992**, (3), 205–213.
[8] Shi Shaoqiu, Yu Bing, Wang Lili, The Thermo-viscoelastic Constitutive Equation of PP and PA Blends and its Rate Temperature Equivalency at High Strain Rates, *Macromolecular Symposia 247*, 1, 28–34. WILEY InterScience. 23 Feb. 2007.

